6-9-2001

Limitations and potential of commercially available rhodamine WT as a groundwater tracer

D. J. Sutton
Duke University

Z. J. Kabala
Duke University

A. Francisco
Duke University

D. Vasudevan
Duke University

WATER RESOURCES RESEARCH, VOL. 37, NO. 6, PAGES 1641–1656, JUNE 2001

Limitations and potential of commercially available rhodamine WT as a groundwater tracer

D. J. Sutton and Z. J. Kabala
Department of Civil and Environmental Engineering, Duke University, Durham, North Carolina

A. Francisco and D. Vasudevan
Nicholas School of the Environment, Duke University, Durham, North Carolina

Abstract. We conducted chemical characterization, batch, column, and modeling studies to elucidate the sorption and transport of rhodamine WT (RWT) in the subsurface. The sand-pack material from the Lizzie field site near Greenville, North Carolina, served as our porous media. Our study confirms earlier results that RWT consists of two isomers with different sorption properties. It also shows that the two isomers have distinct emission spectra and are equally distributed in the RWT solution. The presence of the two isomers with different sorption properties and distinct emission spectra introduces an error in measuring the RWT concentration with fluorometers during porous media tracer studies. The two isomers become chromatographically separated during transport and thus arrive in a different concentration ratio than that of the RWT solutions used for fluorometer calibration and test injection. We found that this groundwater tracer chromatographic error could be as high as 7.8%. We fit six different reactive-solute transport models of varying complexity to our four column experiments. A two-solute, two-site sorption transport model that accounts for nonequilibrium sorption accurately describes the breakthrough curves of the shorter-timescale column experiments. However, possibly due to the groundwater tracer chromatographic error we discovered, this model, or a similar one that accounts for a Freundlich isotherm for one of the solutes, fails to describe the RWT transport in the longer-timescale column experiments. The presence of the two RWT isomers may complicate the interpretation of field tracer tests because a shoulder, or any two peaks in a breakthrough curve, could result from either aquifer heterogeneity or the different arrival times of the two isomers. In cases where isomer 2 sorbs to such an extent that its breakthrough is not recorded during a test, only isomer 1 is measured, and therefore only 50% of the injected mass is recorded. Isomer 1 of RWT can be accurately modeled with a one-solute, two-site, nonequilibrium sorption model. This conclusion and the results from our batch studies suggest that RWT isomer 1 is an effective groundwater tracer but that the presence of isomer 2 hampers its effectiveness.

1. Introduction

Tracer tests have been and continue to be used in subsurface hydrology for aquifer characterization. *Gelhar and Collins* [1971], *Grove and Beetem* [1971], *Welty and Gelhar* [1994], and others have used field tracer tests for determining aquifer dispersivities. In addition, *Pang and Close* [1999], *Adams and Gelhar* [1992], *Hess et al.* [1992], *Mackay et al.* [1986], and others have conducted natural gradient tracer tests for aquifer characterization at Burnham, Canterbury, New Zealand; Columbus Air Force Base, Mississippi; Cape Cod, Massachusetts; and Borden, Ontario, Canada, respectively. Furthermore, two-well tracer tests [*Datta-Gupta et al.*, 1995] and single-borehole tracer tests [*Sutton et al.*, 2000] have also been used for determining spatial variability of hydraulic conductivity.

However, the use of tracers is often complicated by their chemical reactivity and sorption behavior. For physical aquifer characterization the ideal tracer should be conservative and thus should reflect only the effects of the aquifer hydraulic properties on the transport. However, all solutes used in tracer tests react to some degree with the subsurface, resulting in nonconservative transport. Rhodamine WT (RWT), developed in 1966 specifically for use as a general tracer [*Smart and Laidlaw*, 1977], has been used extensively in groundwater studies [e.g., *Pang and Close*, 1999; *Derouane and Dassargues*, 1998; *Pang et al.*, 1998; *Sinton et al.*, 1997; *Ptak and Schmid*, 1996]. This dye is particularly suitable for the following reasons:

1. RWT can be detected at concentrations as low as 0.1 μg L^{-1} using a sensitive fluorometer.
2. RWT is considered the most stable of the fluorescent dyes; sunlight and elemental chlorine are its most significant agents of decay, but they are not present in natural groundwater systems [*Turner Designs*, 1998a].
3. Above pH 6 the fluorescence intensity of RWT is not affected by changes in pH [*Smart and Laidlaw*, 1977].
4. The U.S. Environmental Protection Agency (EPA) does not anticipate adverse health effects when RWT is used as a tracer for water studies if national sanitation guidelines are followed as stated in the *Federal Register* (http://www.epa.gov/ogwdw000/ccl/ccl_fr.txt).
5. *Field et al.* [1995] report that RWT is not an acute toxic

Paper number 2000WR900295.
0043-1397/01/2000WR900295$09.00

threat at or above a specified concentration of 1–2 mg L^{-1} persisting near a groundwater supply for more than 24 hours.

Numerous studies, however, have shown that RWT sorbs both during field-scale groundwater tracer tests [*Ptak and Schmid*, 1996] and laboratory column and batch experiments. *Kasnavia et al.* [1999], *Everts and Kanwar* [1994], *DiFazio and Vurro* [1994], *Soerens and Sabatini* [1994], *Shiau et al.* [1993], *Sabitini and Austin* [1991], *Trudgill* [1987], and *Smart and Laidlaw* [1977] document RWT sorption to a variety of subsurface materials including soil organic matter, clay silicates, and iron oxides, with the extent of sorption varying as a function of the aqueous concentration; the pH, ionic strength, and ionic composition of the solution; and the composition and properties of the solid-matrix. In addition, *Bencala et al.* [1983] found that RWT sorbed to streambed sediments in batch studies.

From their batch studies, *Sabatini and Austin* [1991] concluded that RWT sorbs on to alluvial aquifer sand according to a linear isotherm at low concentrations and a Freundlich isotherm at high concentrations. Also, in their column studies they obtained virtually complete mass recovery, indicating insignificant RWT degradation. In addition, *Sabatini and Austin* [1991] and *Everts and Kanwar* [1994] noted that RWT breakthrough curves are inconsistent with equilibrium sorption of a single solute, suggesting more complicated sorption mechanisms or multiple solutes. *Hofstraat et al.* [1991] isolated two RWT isomers from a commercially available solution and obtained their emission spectra. *Shiau et al.* [1993] also isolated the two RWT isomers and found that they have different sorption properties. The presence of the two isomers offers a possible explanation for the known discrepancy between the measured RWT breakthrough curves and the transport model based on the convection-dispersion equation and equilibrium sorption for a single solute.

Although *Sabatini and Austin* [1991], *Shiau et al.* [1993], *Everts and Kanwar* [1994], and others report equilibrium sorption parameters for RWT, such as partitioning and retardation coefficients, they do not address the kinetics of the sorption. If the timescale of a tracer test is sufficiently short, nonequilibrium sorption will play a significant role in RWT transport. Because the breakthrough curves of tracer tests are often used for estimation of aquifer dispersivities or hydraulic conductivities [e.g., *Datta-Gupta et al.*, 1995; *Sutton et al.*, 2000], the sorption phenomena should be correctly modeled to minimize estimation errors. Transport models that account for nonequilibrium sorption exist [*van Genuchten and Wierenga*, 1976, 1977; *Valocchi*, 1985; *Cameron and Klute*, 1977; *Brusseau et al.*, 1989], but none of them account for two isomers or have been applied to RWT. In some cases, RWT is even considered conservative for simplicity. *Derouane and Dassargues* [1998] assumed the sorption of RWT is negligible according to the findings of *Kass* [1994], who found RWT sorption to be small.

Despite the overwhelming evidence demonstrating that RWT sorbs to subsurface material and contains two isomers, *Pang et al.* [1998] concluded from tracer tests with both RWT and chloride that RWT behaved as a conservative, single-solute tracer during field tests in Burnham, Canterbury, New Zealand. Two other studies that build on the same tracer tests [*Pang and Close*, 1999; *Sinton et al.*, 1997] treated RWT as a conservative tracer.

This study attempts to accurately characterize RWT fate and transport in order to facilitate its use as a tracer for aquifer characterization. Our goal is to evaluate commercially available RWT as a groundwater tracer on a variety of spatial and temporal scales. We evaluate the composition of tracer-grade RWT and its fluorescence properties using standard analytical techniques (high-pressure liquid chromatography (HPLC) with UV and fluorescence detection), the sorption phenomena of each isomer in batch studies, and the transport of each isomer in column experiments. We examine existing transport models and develop models to account for the two isomers of RWT and their sorption at various timescales. Results from the batch sorption studies and chemical analyses of RWT are utilized in model evaluation and development. We expect such a model to improve the interpretation of two-well and single-borehole RWT tracer tests conducted on relatively short timescales.

2. Materials and Methods

The RWT used in this study was obtained from Turner Designs, Inc. (Sunnyvale, California), lot number A97B015, with a concentration specified as 21.33% ± 2.5% and specific gravity 1.2 ± 0.1. In this study, concentrations of RWT refer to the concentration of the active ingredient, not the solution of 21.33% active ingredient. The chemical characterization studies and batch studies employ deionized (DI) water (MILLIQ, Millipore, Inc.). With the exception of the DI water used for diluting the original RWT solution by a factor of 10^{-3}, all water used in the column study is tap water left open to the atmosphere for more than 3 days to allow the chlorine to degas. The pH of the degassed tap water is approximately 6.7–7.0.

The water used for zeroing and calibrating the fluorometer was obtained by collecting the degassed water after it passed through the media-filled column. We should note that a 100-ppb RWT solution prepared with tap water that is not allowed to degas shows a reduction in apparent concentration to approximately 30 ppb in less than 1 day. We are not yet sure whether there is a loss in RWT fluorescence due to the presence of chlorine or whether another constituent in the water causes RWT degradation. However, in multiple experiments, after the tap water was opened to the atmosphere for 3 days and then used to prepare a 100-ppb sample of RWT, no significant reduction was observed.

The subsurface material chosen for these experiments is a sample of the medium used in the sand packs of monitoring wells L-35, L-36, and L-39 at the Lizzie field site near Greenville, North Carolina. Its porosity is $\theta = 0.40$, and its bulk density is $\rho_b = 1.40$ g cm^{-3}. This material was chosen for its relative simplicity and its relevance to tracer tests conducted in those wells [*Sutton et al.*, 2000]. Although not representative of aquifer material at the Lizzie field site, it is in the skin zones there, and a significant portion of RWT travels through this skin zone material.

2.1. Chemical Characterization of Tracer-Grade RWT

Chemical constituents of a 15-ppm solution from a commercially obtained RWT mixture were separated using HPLC with UV diode array detection (HP, 1100 Series). Separation was achieved using an Eclipse XDB-C18, 150 × 4.6 mm column (HP, Zorbax) as the immobile phase and a solution of 65% methanol (Mallinckrodt) and 35% 5×10^{-3} *M* phosphoric acid (pH 3.5) as the mobile phase. The separated constituents of the RWT mixture were collected (Eldex Universal fraction collector) and subsequently analyzed for fluorescence at an excitation wavelength of 535 nm and an emission wavelength

of 590 nm (HCS 7000 BioAssay Fluorescence and Absorption Plate Reader, Perkin Elmer). For eluent fractions exhibiting fluorescence, emission spectra were obtained by scanning fluorescence between 500 and 800 nm while excitation wavelength was held constant at 555 nm (LS-50B Luminescence Spectrophotometer, Perkin Elmer).

2.2. Batch Studies

Sorption of tracer-grade RWT onto untreated and treated (with H_2O_2 oxidation to remove organic matter) sand-pack materials was examined at pH 7 as a function of RWT concentration (100 ppb to 7 ppm) and time. Analyzing RWT sorption to the treated and untreated sand allows us to evaluate the sorption of RWT onto both silica and organic matter. Sand-pack material and DI water containing 10^{-2} *M* NaCl were added to aluminum foil wrapped 25-mL amber vials with Teflon septa to obtain a solids loading of 500 g L^{-1}. The slurry was allowed to equilibrate for 30 min at 25°C in an orbital shaker (LabLine, Model 3540) and was then spiked with a known concentration of tracer-grade RWT. The suspension was set to pH 7 using small volumes of concentrated HCl or NaOH. NaCl and HCl/NaOH solutions were added to DI water in order to simulate the conductivity and pH of the tap water utilized in the column experiments. The samples were continuously shaken and equilibrated in a darkened hood for the duration of the experiment. An aliquot of the supernatant was removed and filtered with a 0.22-μm membrane filter. The RWT isomers in the filtered aliquot were separated by HPLC, and their respective concentrations were ascertained from UV absorbance at 256 nm (for initial RWT concentrations above 1 ppm) or fluorescence at an excitation wavelength of 555 nm and an emission wavelength of 580 nm (for initial RWT concentrations below 1 ppm). The mass sorbed was calculated as loss from bulk solution by subtracting the concentrations recovered in the supernatant from the initial isomer concentrations in the reactor. In all cases, desorption experiments were performed to confirm that loss from bulk solution was due to sorption alone. At the end of the sorption experiments all of the supernatant was removed from the reactor, methanol was added to solid matrix, allowed to equilibrate for 30 min, and concentration of RWT constituents in the methanol was ascertained.

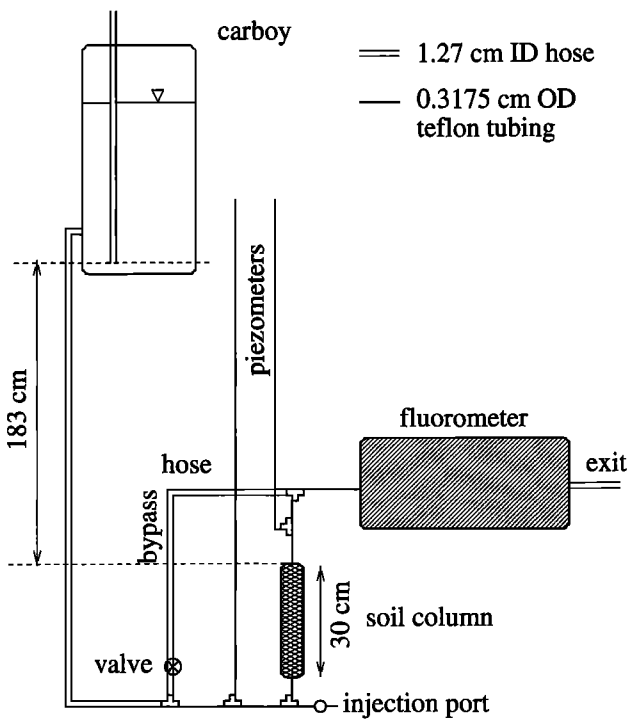

Figure 1. Schematic of the laboratory column and the fluorometer.

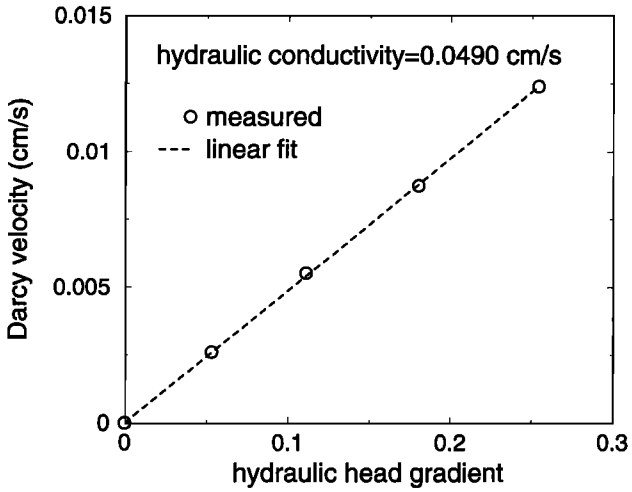

Figure 2. Relationship of flow rate to hydraulic head differential in the piezometers on either side of the column.

2.3. Column Studies

A schematic of our column system with dimensions is shown in Figure 1. The system provides a constant head of up to 183 cm. It utilizes a Fisher Scientific borosilicate glass column with a 2.4-cm radius and a length of 30 cm. The portions of the system between the injection port and the column and between the column and the fluorometer consist of 0.125-inch OD Teflon tubing and fittings. Two piezometers are placed on either side of the column to determine the head differential and, via Darcy's law, the hydraulic conductivity of the media in the column. A bypass hose circumventing the column can provide additional flow to reduce the heating of the sample as it travels through the fluorometer. When auxiliary flow is not used, the flow rate exiting the system is equal to that in the column and is measured volumetrically with a graduated cylinder and a stopwatch. When auxiliary flow is used, the flow rate exiting the system is higher than that through the column, and therefore the flow rate through the porous media is estimated via Darcy's law using the previously measured hydraulic conductivity and the head differential provided by the piezometers. Figure 2 shows the hydraulic conductivity estimate for the column from one of our column experiments (experiment 4). The correlation coefficient of the linear fit is greater than 0.99.

We measured the concentration of RWT with a Turner Designs Model 10-AU field fluorometer capable of detecting concentrations of RWT from 0.1 to 100 ppb [*Turner Designs*, 1998b]. The light source is a clear quartz lamp, the reference filter is a longwave 535-nm square sharp-cut filter, the excitation filter is a 550-nm interference narrow band-pass filter, and the emission filter is a 570-nm longwave sharp-cut filter, which allows transmission of light with a wavelength above 570 nm.

We conducted four separate column experiments all using the same sample of sand. Table 1 shows the linear pore-scale

Table 1. Parameters for Four Column Experiments

Experiment	c_i, ppb	V_i, cm^3	v, cm s^{-1}	L/v, min
1	21.3	1.0 mL	0.193	2.6
2	213	0.93 mL	0.129	3.9
3	8.53×10^3	1.0 mL	0.0175	28.6
4	8.53×10^3	1.0 mL	0.0117	42.7

Parameters are injection concentration, c_i; injection volume, V_i; linear pore-scale velocity, v; and travel time, L/v, where L is the length of the column.

velocity (specific discharge divided by the porosity), injection concentration of RWT, and injection volume for each test. Because of the low flow rates, column experiments 3 and 4 required auxiliary flow to prevent the sample from heating significantly as it passed through the fluorometer sample cell.

3. Laboratory Results

3.1. Chemical Characterization of Tracer-Grade RWT

The separation of constituents of the RWT mixture by HPLC and analysis for UV absorption is depicted in Figure 3; the chromatogram shows three unique UV spectra, reflective of three compounds present in RWT. Analysis of eluent fractions corresponding to each of three peaks revealed that only the compounds found in peaks two and three (hereinafter referred to as isomers 1 and 2) exhibited fluorescence at an excitation wavelength of 535 nm and an emission wavelength of 590 nm. This suggests that tracer-grade RWT consists of one inactive ingredient, possibly an impurity, and two active ingredients, possibly isomers of RWT. It may be noted that the two RWT isomers have similar but distinct UV spectra. As mentioned earlier, the detection of two RWT isomers is consistent with previous studies by *Hofstraat et al.* [1991] and *Shiau et al.* [1993]. Individual isomers may differ in structure with respect to the position of the carboxylic acid groups on the aromatic ring shown in Figure 4; spectroscopic analyses, not done as part of this study, are required to identify the exact structure of the three constituents.

As shown in Figure 5, at pH 3.4 and an excitation wavelength of 555 nm, the two isomers of RWT have relatively similar yet

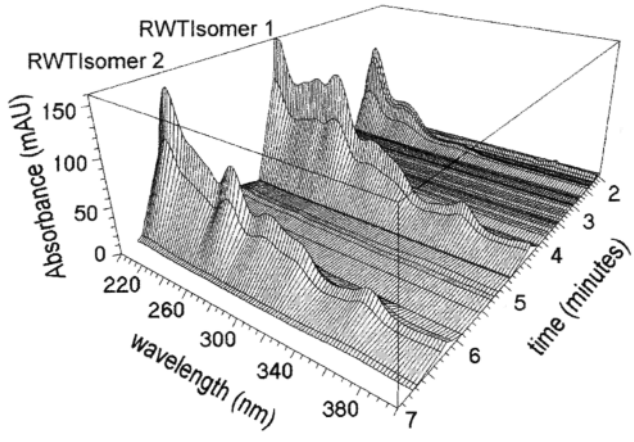

Figure 3. Separation of UV active constituents in the tracer-grade rhodamine WT (RWT) mixture by high-pressure liquid chromatography (HPLC) and UV spectra as obtained from a diode array detector.

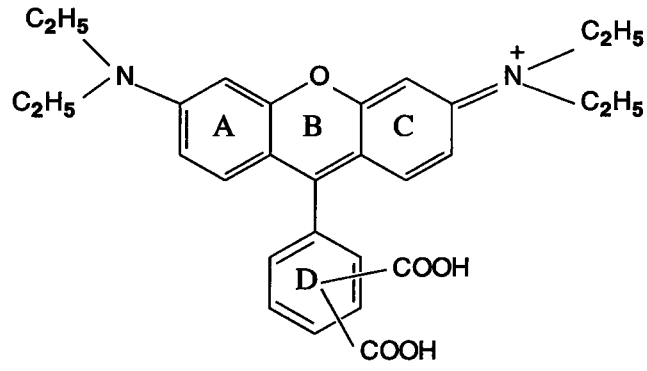

RHODAMINE WT

Figure 4. Molecular structure of RWT (adapted from *Smart and Laidlaw* [1977]). The lines connecting the carboxylic acid groups to the center of aromatic ring D signify that the positions of these groups are either unknown or may vary. Differences in the positioning of the two carboxylic acid groups may account for the structural differences in the two isomers. The ABC-conjugated ring system is the fluorophore responsible for fluorescence of both RWT isomers.

shifted emission spectra with nearly identical emission intensities at their respective maxima. The spectra shown in Figure 5 were obtained with the Perkin Elmer luminescence spectrometer, Model LS-50B, which has an accuracy of ±1.0 nm and a repeatability of ±0.5 nm. Thus the location of the emission maxima may have a ±1.0-nm bias, but the shift of approximately 3 nm at the peaks (and 8 nm around wavelength 625 nm) is real due to the high degree of repeatability. With an Agilent Technologies, 1100 Series fluorescence detector, we confirmed that this shift in the spectra also exists at pH 7.0. Given that both isomers have the same fluorophores (xanthene rings, labeled A, B, and C in Figure 4), a similarity in their emission intensities at the respective maxima suggests that the two isomers are equally distributed (a 50/50 ratio) in the trac-

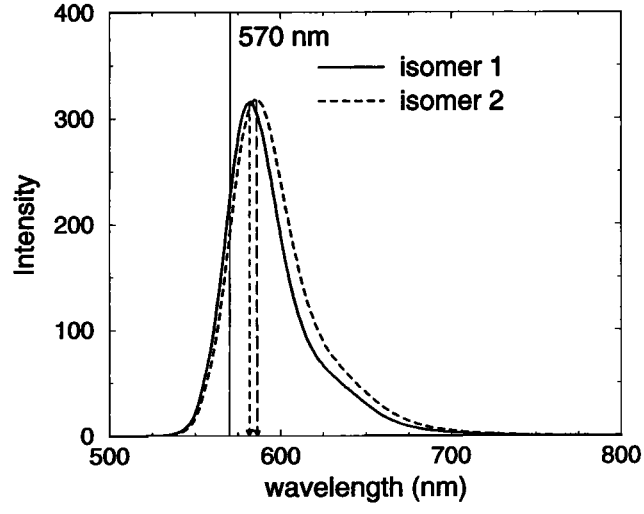

Figure 5. Emission spectra for isomers 1 and 2 at an excitation of 555 nm. The emission maxima for isomer 1 is at 585 nm, and that for isomer 2 is at 588 nm. The Turner Designs Model 10-AU field fluorometer measures the light at wavelengths longer than 570 nm.

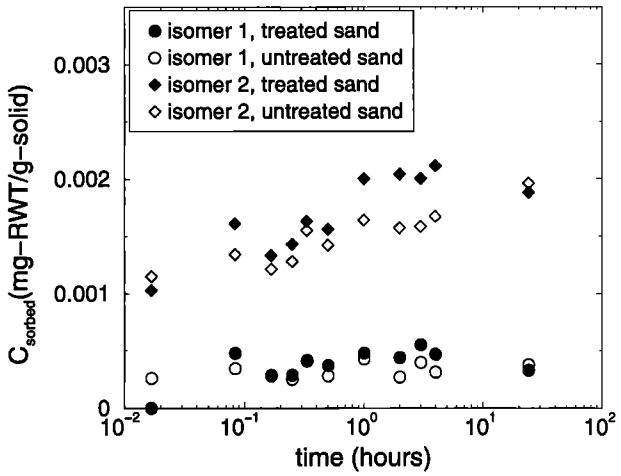

Figure 6. Sorption of isomer 1 and isomer 2 onto untreated and treated sand-pack material as a function of time. Solids loading is 500 g L^{-1}; pH is 7; [NaCl] = 10^{-2} M; and $[RWT]_{initial}$ = 6 ppm, active ingredient.

er-grade mixture. Our preliminary proton nuclear magnetic resonance (NMR) tests appear to confirm this ratio.

Our estimate of a 50/50 distribution differs from that previously reported in the literature. *Shiau et al.* [1993] determined that the tracer-grade RWT contains 40% by weight isomer 1 and 60% by weight isomer 2 based on column experiments with select aquifer material and RWT detection using a Turner Model 110 fluorometer. For this methodology to be accurate, the emission spectra of isomers 1 and 2 would have to be identical. Figure 5 shows that these emission spectra are distinct between 500 and 700 nm. Hence the 40–60% weight distribution determined by *Shiau et al.* [1993] may in part reflect differences in the fluorescence characteristics of the two isomers and not the true weight percent composition of the two isomers in their RWT mixture.

3.2. Batch Studies

H_2O_2 treatment is expected to successfully remove most of the organic matter, and hence we assume that the treated sand represents a mineral (silica) surface while the untreated sand represents a mineral (silica) surface with patches of organic matter. Figure 6 shows that isomer 1 sorption onto the treated and untreated sand achieves sorption equilibrium in a matter of minutes. It is also evident that between 1 and 2 hours, isomer 2 is in equilibrium sorption to the treated sand. However, after the plateau at approximately 1 hour, we observe a significant increase in the sorption of isomer 2 on untreated sand between 3 and 24 hours. Although beyond the scope of this study, additional experiments are needed to determine the time to equilibrium for isomer 2 sorption onto untreated sand. On the basis of our observations we conclude that isomers 1 and 2 exhibit different kinetics of sorption onto the untreated sand-pack material.

As seen in Figure 7, isomer 2 sorbs to a greater extent onto both the treated and untreated sand-pack material than does isomer 1. While isomer 2 sorbs to almost equal extents to both the treated and untreated sand, isomer 1 does not. The partitioning coefficient for isomer 1 sorption onto untreated sand is greater than that onto treated sand by a factor larger than 1.5. Therefore it appears that the organic matter content of these solids does not significantly increase the sorption of isomer 2 but that it does have a small effect on the sorption of isomer 1. Hence processes other than hydrophobic exclusion from bulk solution are likely to influence the nature and extent of RWT isomer sorption. On the basis of these observations we infer that the sand-pack material affords two types of sorption sites: a silica surface and patches of organic matter. We also infer that the two isomers sorb to these surfaces with distinct rates and mechanisms of interaction.

We fit Freundlich isotherms

$$C_{sorbed} = K_d C^n_{aqueous} \quad (1)$$

to all sets of data presented in Figure 7 and summarize the results in Table 2. For the sorption of isomer 1 onto treated and untreated sand, $n \approx 1$, as demonstrated in Table 2. Linearization of these isotherms results in an increase of the sum of squares error by approximately 1–2%. We therefore adopt the linearized isotherm for isomer 1.

As mentioned earlier, we conducted desorption experiments using methanol as an extractant. While we were able to successfully desorb isomer 1 from the treated and untreated sand, we were unable to completely recover isomer 2 from either matrix. Thus isomer 2 sorbs more strongly than does isomer 1. Multiple extractions with methanol or the use of alternative

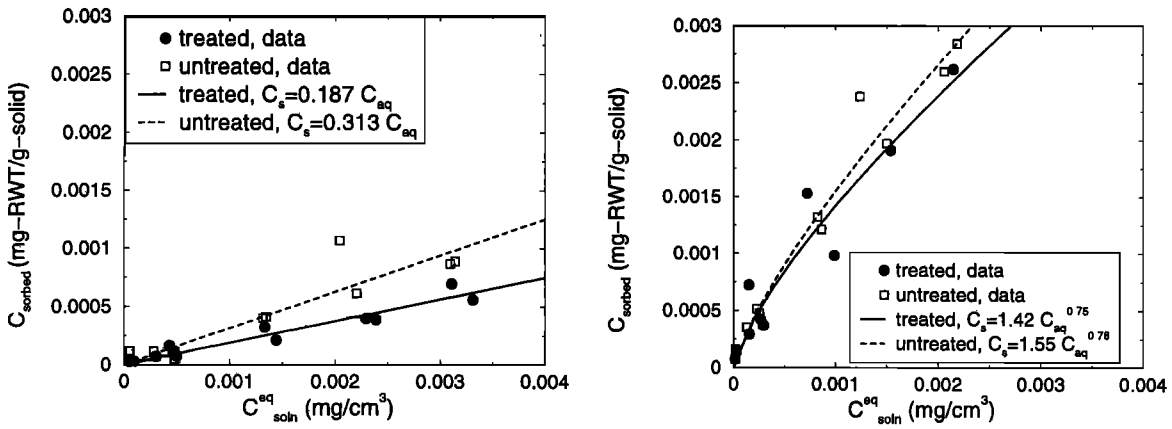

Figure 7. Sorption of (a) isomer 1 and (b) isomer 2 onto untreated and treated sand-pack material. Initial RWT concentration range is 1 ppb to 12 ppm, active ingredient. Solids loading is 500 g L^{-1}, pH is 7, [NaCl] = 10^{-2} M, and equilibration time is 24 hours.

Table 2. Estimated Partitioning Coefficients and Exponents for a Freundlich Isotherm Fitted to the Batch Experiment Data

	Freundlich Isotherm, Isomer 1		Linearized Isotherm, Isomer 1		Freundlich Isotherm, Isomer 2	
	Treated	Untreated	Treated	Untreated	Treated	Untreated
K_d, cm^3 g^{-1}	0.198	0.342	0.187	0.313	1.42	1.55
n	0.94	0.90	1.0	1.0	0.75	0.78

extractants such as methylene chloride or a 10^{-3} M NaF solution of pH 4 would be required to successfully desorb isomer 2.

3.3. The RWT Chromatographic Error

The Turner Designs Model 10-AU fluorometer measures the concentration of RWT by exciting the sample solution with 550-nm-wavelength light, measuring the emitted light at wavelengths above 570 nm and converting the intensity of the emitted light to concentration based on a linear calibration curve obtained with standard solutions of the commercial-grade dye [*Turner Designs*, 1998b]. However, Figure 5 shows that the emission spectra of RWT isomers 1 and 2 are different at wavelengths above 570 nm when excited by light with a wavelength of 555 nm. Because the isomers emit differently, the relationship of fluorescence to concentration for each isomer also is different. The average intensity $\bar{I}$ of light emitted by a given isomer between 570 and 800 nm can be calculated by

$$\bar{I} = \frac{1}{800 - 570} \int_{570}^{800} I(\lambda)\, d\lambda, \qquad (2)$$

where $I(\lambda)$ is the intensity of emitted light from a given isomer as a function of wavelength. The average intensities for isomers 1 and 2 between 570 and 800 nm are 55.8 and 65.2, respectively. Therefore, for equal concentrations of the two isomers in the sample chamber of the Turner Designs Model 10-AU fluorometer, 46.1% of the light intensity is due to isomer 1 and 53.9% is due to isomer 2 assuming the original solution is a 50/50 mixture of isomer 1 and isomer 2.

Using a fluorometer calibrated with a solution made from the commercially available dye, if the ratio of the concentration of isomer 1 to that of isomer 2 remains the same between the calibration and sampling, then the concentration measurements will be accurate. However, because of the different sorption properties of isomers 1 and 2 (Figures 6 and 7), the transport of RWT through porous media will produce a chromatographic effect, separating the two isomers. Therefore the ratio of the two isomers will change as the RWT solution travels through the porous media because isomer 1 will travel faster than isomer 2. Because the emission intensity from a sample concentration of isomer 1 is lower than that from the same concentration of the commercially available dye used for the calibration, the concentration of isomer 1 will be underestimated. Similarly, the concentration of isomer 2 will be overestimated. If during a tracer test the sample water contains a given concentration of RWT that is nearly 100% isomer 1 and 0% isomer 2, assuming a 50/50 isomer ratio, the light intensity will only be 92.2% of what is expected for that concentration. Because of the linear relationship between emission intensity and RWT concentration (for concentrations of up to 0.1 ppm) [*Turner Designs*, 1998b], one may expect to underestimate the RWT concentration by up to 7.8%. (Likewise, if the sample chamber contained nearly 100% isomer 2, one may expect to overestimate the RWT concentration by 7.8%.) Hereinafter we use the term chromatographic error to refer to the error introduced by the separation of tracer-grade RWT into its constituent isomers, each with distinct emission spectra.

3.4. Column Studies

As demonstrated above, using a tracer that has two isomers with different emission spectra and different sorption properties imposes limits on the accuracy of RWT concentrations measured using field fluorometers, such as the Turner Designs Model 10-AU field fluorometer used in our column experiments. To fully explore the benefits and limitations of using the Turner Designs Model 10-AU fluorometer, we initially assume that the fluorometer accurately measures RWT concentration and later discuss the errors from these assumptions.

To present the column experimental data in dimensionless form, we introduce the dimensionless time $T = vt/L$; dimensionless distance $Z = z/L$; and dimensionless concentration

$$C(Z, T) = c(z, t)/C_0, \qquad (3)$$

where $c(z, t)$ is the flux concentration in physical space z and time t; and $C_0 = M/(V\theta)$, where M is the mass of tracer injected, V is the volume of the column, and θ is the porosity. We note that the dimensionless concentration $C(Z, T)$ is normalized so that the total mass under the breakthrough curve is equal to 1 if full mass recovery is achieved.

The breakthrough curves, $C(1, T)$, from all four column experiments (Table 1) are shown in Figure 8. We introduce the notation BTC_i to denote the breakthrough curve associated with column experiment i. As is apparent, BTC1 and BTC2, which result from experiments conducted at the higher flow rates, are almost identical in their dimensionless form. However, a shoulder is evident in BTC3, and a second peak is evident in BTC4. Analysis of the data from the four column runs suggests a mass recovery of approximately 80%; therefore about 20% of the injected mass was not recovered in each study. As mentioned earlier, we know from observation that the water used in the system does not affect the fluorescence of the RWT over the course of days. Thus the missing mass must have remained sorbed to the material or have diffused into immobile regions and returned to the main flow at a rate too small to result in a detectable concentration. Additionally, recovering all of the mass of isomer 2 from the batch studies was difficult while recovering all of the mass of isomer 1 was not. Therefore this missing mass should consist mostly of isomer 2.

To confirm the hypothesis that the missing mass results from slow desorption of RWT from the column material and not quenching of the fluorescence, we stopped the flow after obtaining BTC2 to allow time for the mass to desorb. We then

restarted the flow to extract this desorbed mass. We began by stopping the flow for 10 min. When we restarted it we observed RWT leaving the column. We repeated this procedure three times, each time recording additional mass. Over the course of 8 days, we used a similar procedure with the stopping periods ranging from 2 to 24 hours. We then repeated the procedure twice with stopping times of 11 and 4 days. The breakthrough curve and the mass recovered over this 24-day period accounted for 90% of the injected mass. Although we stopped the flow on the 24th day, we suspect the column contained the remaining 10% of RWT mass. The drift in the calibration of the fluorometer is less than 0.5% per month [*Turner Designs*, 1998b] and therefore should not have biased the mass recorded over these 24 days.

4. Modeling

We consider six different models to fit our experimental column data. The first three models treat RWT as a single-solute sorbing tracer that interacts with one to four types of sorbing sites. The other three models account for the two fluorescing isomers of RWT, and we assume that they are not interacting with each other or competing for surface sites. The first two-isomer model assumes a linear isotherm (equation (1) with $n = 1$) and provides one type of sorbing site for each isomer. The second two-isomer model also assumes a linear isotherm but provides two types of sorbing sites for each isomer, one where RWT sorbs instantaneously and the other where RWT sorption is governed by first-order kinetics. The third two-isomer model also provides two-sorption sites for each isomer, but for isomer 2 it assumes a Freundlich isotherm (equation (1) with n not necessarily equal to 1) for one of the sites. To conveniently denote each model, we introduce the notation Mij, where i represents the number of solutes and j represents the number of sorbing sites for each solute. M22* denotes the two-isomer model that incorporates nonlinear sorption.

For each model we use the dimensionless forms C, T, and L described earlier and assume a Dirac-delta impulse injection, $\delta(T)$, at the entrance of the column (a valid assumption as long as the duration of the injection is much shorter than the timescale of the tracer transport through the column), no tracer in the eluting water or sorbed to the material at the initial time, and a semi-infinite spatial domain. We invoke the latter assumption because it leads to simpler models; although our column is of finite rather than infinite length, we observe (measure) the plume at the distance L ($Z = 1$) from the injection end of the column, and what happens beyond it is of no concern.

All of the models with the exception of those assuming a single equilibrium sorption site or nonlinear sorption are solved in the Laplace domain and inverted using the *Talbot* [1979] algorithm. Because there are no complex singularities in the Laplace domain solutions, we set the parameters defined by *Talbot* [1979, case 1, equation (68)] to $\nu = 1$, $\sigma = \sigma_o$, and $\tau = \omega_T = \lambda T$, where λ is a parameter that scales the time and Laplace domain variables. *Talbot* [1979] states that the value of τ varies with the problem, but we have found through experimentation that $\tau = \omega_T = 16$ is sufficient. We also found that $n_c = 191$ points in the complex plane is sufficient.

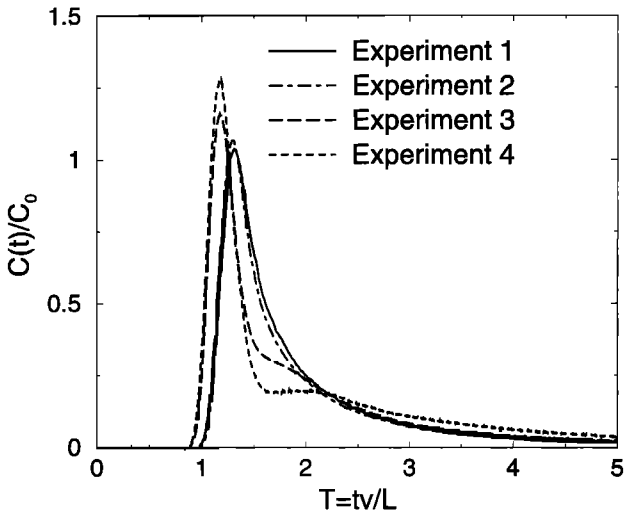

Figure 8. The breakthrough curves from all four column experiments. Dimensionless concentration is plotted against dimensionless time. Small-amplitude noise is noticeable in the later, more level portion of the breakthrough curve from experiment 4. Although present with the same magnitude throughout the breakthrough curve, this noise is not apparent on the peak because it aligns more closely with the steeper slopes.

4.1. M1*i* Models

4.1.1. Model M11: Single-solute transport, equilibrium sorption sites. This simplest, well-documented model [*Jury et al.*, 1991], based on the convection-dispersion equation with equilibrium sorption model, is described in dimensionless form as the following initial-boundary-value problem (IBVP):

$$R\frac{\partial C}{\partial T} = \frac{1}{P}\frac{\partial^2 C}{\partial Z^2} - \frac{\partial C}{\partial Z} \tag{4}$$

subject to

$$C(Z, T = 0) = 0 \tag{5}$$

$$C(Z = 0, T) = \delta(T) \tag{6}$$

$$C(Z = \infty, T) = 0, \tag{7}$$

where R is the retardation coefficient

$$R = 1 + \frac{\rho K_d}{\theta}, \tag{8}$$

where ρ and θ are the known bulk density and porosity of the porous media, respectively; K_d is the partitioning coefficient of the tracer to the porous media; $P = vL/D$ is the Peclet Number; and D is the dispersion coefficient.

4.1.2. Model M12: Single-solute transport, equilibrium and nonequilibrium sorption sites. The next model, described by *Selim et al.* [1976], *van Genuchten and Wierenga* [1976, 1977], and others, assumes two types of sorption sites, one governed by equilibrium sorption and the other governed by nonequilibrium sorption. *Nkedi-Kizza et al.* [1984] expressed the model in dimensionless form as the following IBVP:

$$\beta R\frac{\partial C}{\partial T} + (1-\beta)R\frac{\partial S}{\partial T} = \frac{1}{P}\frac{\partial^2 C}{\partial Z^2} - \frac{\partial C}{\partial Z} \tag{9}$$

$$(1 - \beta)R \frac{\partial S}{\partial T} = \omega(C - S) \tag{10}$$

subject to

$$S(Z, T = 0) = 0 \tag{11}$$

and (5)–(7). In addition,

$$\beta = \frac{\theta + F_e \rho K_d}{\theta + \rho K_d} \tag{12}$$

$$\omega = k(1 - F_e)\rho K_d L/q \tag{13}$$

$$S = \frac{s}{(1 - F_e)K_d C_0}. \tag{14}$$

F_e is the fraction of solute in equilibrium sorption, K_d is the partitioning coefficient for both sorption sites, k is a first-order rate coefficient for the nonequilibrium sorption, q is the Darcy velocity, s is the time- and space-varying mass fraction of sorbate to sorbent, and all other parameters are defined earlier. We note that this two-site sorption model is mathematically equivalent to the physical nonequilibrium model in which solute partitions into and out of immobile zones [*van Genuchten and Wierenga*, 1976, 1977]; however, we consider only the sorption version because of the known RWT chemical sorption properties. Also, we note that for $\beta = 1$ this model reduces to the previous model, M11. The four parameters to be estimated are β, R, ω, and P.

4.1.3. Model M14: Single-solute transport, mobile and immobile zones each with equilibrium and nonequilibrium sorption sites. The third model is proposed by *Brusseau et al.* [1989] and has eight fitting parameters. Four sites for sorption are assumed, a site governed by chemical equilibrium and another governed by chemical nonequilibrium in both mobile and immobile zones of the medium. The model can be expressed in dimensionless form as the following IBVP:

$$R_{m1} \frac{\partial C_m}{\partial T} + R_{m2} k_m (C_m - S_m^*) + \omega_b (C_m - C_{im}) = \frac{1}{P} \frac{\partial^2 C_m}{\partial Z^2} - \frac{\partial C_m}{\partial Z} \tag{15}$$

$$R_{im1} \frac{\partial C_{im}}{\partial T} + R_{im2} k_{im} (C_{im} - S_{im}^*) = \omega_b (C_m - C_{im}) \tag{16}$$

subject to

$$C_m(Z, T = 0) = C_{im}(Z, T =) = 0$$
$$S_m^*(Z, T = 0) = S_{im}^*(Z, T) = 0 \tag{17}$$

$$C_m(Z = 0, T) = \delta(T) \qquad C_{im}(Z = 0, T) = 0 \tag{18}$$

$$C_m(Z = \infty, T) = C_{im}(Z = \infty, T) = 0, \tag{19}$$

where C_m and C_{im} are the dimensionless aqueous concentrations of the solute in the mobile and immobile zones, respectively; ω_b is a first-order mass transfer coefficient nondimensionalized by scaling with the pore-scale velocity v and the length of the column L; and k_m and k_{im} are the first-order rate constants for nonequilibrium sorption in mobile and immobile zones nondimensionalized with the same scaling. $S_m^* = S_m/((1 - F_m)K_{dm}C_o)$, where S_m is the ratio of the mass of sorbate in chemical nonequilibrium in the mobile zone to the mass of sorbent in the mobile zone, F_m is the fraction of sorbent in the mobile zone associated with instantaneous sorption, and K_{dm} is the equilibrium partitioning coefficient in the mobile zone. Analogously, $S_{im}^* = S_{im}/((1 - F_{im})K_{dim}C_o)$, where the subscript "im" denotes the immobile zone. In addition,

$$R_{m1} = \phi + \frac{F\rho}{\theta} F_m K_{dm} \tag{20}$$

$$R_{m2} = \frac{F\rho}{\theta} (1 - F_m) K_{dm} \tag{21}$$

$$R_{im1} = 1 - \phi + \frac{(1 - F)\rho}{\theta} F_{im} K_{dim} \tag{22}$$

$$R_{im2} = \frac{(1 - F)\rho}{\theta} (1 - F_{im}) K_{dim} \tag{23}$$

are retardation coefficients; $\phi = \theta_m/\theta$ is the ratio of the mobile zone porosity to the total porosity; F is the mass fraction sorbent comprising the mobile zone; and the other parameters are already defined. The fitting parameters are R_{m1}, R_{m2}, R_{im1}, R_{im2}, k_m, k_{im}, ω_b, and P.

4.2. M2*i* Models

To account for the two isomers of RWT, we combine various M1*i* models into M2*i* models.

4.2.1. Model M21: Two solutes, equilibrium sorption sites. For two isomers in equilibrium sorption the dimensionless IBVP problem is given by

$$R_1 \frac{\partial C_1}{\partial T} = \frac{1}{P} \frac{\partial^2 C_1}{\partial Z^2} - \frac{\partial C_1}{\partial Z} \tag{24}$$

$$R_2 \frac{\partial C_2}{\partial T} = \frac{1}{P} \frac{\partial^2 C_2}{\partial Z^2} - \frac{\partial C_2}{\partial Z} \tag{25}$$

$$C_1(Z, T = 0) = C_2(Z, T = 0) = 0 \tag{26}$$

$$C_1(Z = 0, T) = f\delta(T) \qquad C_2(Z = 0, T) = (1 - f)\delta(T) \tag{27}$$

$$C_1(Z = \infty, T) = C_2(Z = \infty, T) = 0, \tag{28}$$

where

$$C(Z, T) = C_1(Z, T) + C_2(Z, T) \tag{29}$$

is the total solute concentration and the subscripts 1 and 2 refer to isomers 1 and 2, f is the fraction of the RWT that is isomer 1, and C_1 and C_2 are the dimensionless flux concentrations of the two isomers normalized by the total injection mass (i.e., the sum of the isomer injection masses). The fitting parameters for this model are R_1, R_2, P, and f.

4.2.2. Model M22: Two solutes, equilibrium and nonequilibrium sorption sites. Using model M12 to describe each isomer yields M22, which is described by the following IBVP:

$$\beta_1 R_1 \frac{\partial C_1}{\partial T} + (1 - \beta_1) R_1 \frac{\partial S_1}{\partial t} = \frac{1}{P} \frac{\partial^2 C_1}{\partial Z^2} - \frac{\partial C_1}{\partial Z} \tag{30}$$

$$(1 - \beta_1) R_1 \frac{\partial S_1}{\partial t} = \omega_1 (C_1 - S_1) \tag{31}$$

$$\beta_2 R_2 \frac{\partial C_2}{\partial T} + (1 - \beta_2) R_2 \frac{\partial S_2}{\partial t} = \frac{1}{P} \frac{\partial^2 C_2}{\partial Z^2} - \frac{\partial C_2}{\partial Z} \tag{32}$$

$$(1 - \beta_2)R_2 \frac{\partial S_2}{\partial t} = \omega_2(C_2 - S_2) \tag{33}$$

subject to

$$S_1(Z, T = 0) = S_2(Z, T = 0) = 0 \tag{34}$$

and (26)–(28). Again, (29) represents the total solute concentration, and

$$\beta_i = \frac{\theta + F_{ei}\rho K_{di}}{\theta + \rho K_{di}} \tag{35}$$

$$\omega_i = k_i(1 - F_{ei})\rho K_{di} L/q \tag{36}$$

$$S_i = \frac{s_i}{(1 - F_{ei})K_{di}C_0}, \tag{37}$$

where $i = 1$ or 2 for isomer 1 or 2 and the other parameters are defined in the description of M12. The fitting parameters are β_1, β_2, R_1, R_2, ω_1, ω_2, P, and f.

4.2.3. Model M22*: Two solutes, equilibrium and nonequilibrium sorption sites, isomer 2 follows a nonlinear Freundlich isotherm. The IBVP for this model is equivalent to that of M22 with the exception that (33) is replaced with

$$(1 - \beta_2)R_2 \frac{\partial S_2}{\partial t} = \omega_2(C_2^{n_2} - S_2), \tag{38}$$

where n_2 is an empirically determined parameter of the Freundlich isotherm. For $n_2 = 1$ this model reduces to M22. However, in addition to fitting the eight parameters from M22, we are also fitting n_2. We solved this IBVP with a fully implicit finite difference scheme approximating (27) with

$$C_1(Z = 0, 0 \le T \le \Delta T) = \frac{f}{\Delta T}$$
$$C_2(Z = 0, 0 \le T \le \Delta T) = \frac{1 - f}{\Delta T} \tag{39}$$

and approximating (28) with

$$C_1(Z = 2, T) = C_2(Z = 2, T) = 0. \tag{40}$$

We confirmed the convergence and accuracy of this model by comparing results from it with $n_2 = 1$ to the results from M12 calculated with the same parameters. The model converges for $\Delta T = 5 \times 10^{-4}$ and $\Delta Z = 0.01$.

5. Parameter Estimation

The nonlinear minimization problems for obtaining the least squares fits of the models to the data are solved using a modification of the Levenberg-Marquardt algorithm from the Minpack Project [*Garbow et al.*, 1980]. While only one global least squares fit should exist, many local minima may exist. In fitting each model to each data set, we began the minimization process with a variety of initial guesses in an attempt to find the global minimum; however, we cannot guarantee that our parameter estimates represent the global least squares fit. For each model fit we report a fitting error E, which we determine from the following formula:

$$E = \frac{1}{N}\sum_{i=1}^{N} (C(1, T_i) - \bar{C}_i)^2, \tag{41}$$

where $\bar{C}_i$ is the ith concentration point in a data set, $C(1, T_i)$ is the concentration at the end of the column calculated by the model at the corresponding dimensionless time, and N is the number of the concentration point in a measured breakthrough curve at which $\bar{C}_i \approx \bar{C}_p/100$, where $\bar{C}_p$ is the peak concentration of the measured breakthrough curve.

5.1. M1*i* Results

Figure 9a shows the least squares fit of M11 to BTC1, $E \approx 0.01$. Fitting M11 to BTC2 yields similar results (not shown). The M11 model fits both breakthrough curves poorly.

The least squares approximation of M12 to BTC1 is shown in Figure 9b. The results for fitting M12 to BTC2 are similar (not shown), which is expected given the similarity of the two breakthrough curves. $E \approx 0.002$ for both data sets, and visual inspection confirms that M12 more accurately describes the RWT transport than M11. However, significant differences remain between the measured and modeled breakthrough curves. While the two-site model simulates the peak well, it overestimates the mass between $T \ge 2.5$ and $T \le 7.5$. The data suggest that this mass is still sorbed to the material and exits the column later at concentrations too low to measure.

M14 describes the transport of a solute that is affected both by physical partitioning of the tracer between mobile and immobile zones and chemical sorption. Its fit to BTC1 is shown in Figure 9c. Once again, given the similarities between BTC1 and BTC2 (not shown), the fits are similar with $E \approx 1 \times 10^{-4}$ for both data sets. Despite the excellent visual fit, the retardation coefficient of the solute that is in equilibrium sorption within the immobile phase is $R_{im1} = -2 \times 10^{-4}$ from the BTC1 fit and $R_{im1} = 0.37$ from the BTC2 fit. The estimates of R_{im1} from both experiments are unreasonable; a value less than one, and especially less than zero, is unrealistic for a retardation coefficient, as it suggests that the partitioning coefficient is negative.

The outcome of the M1*i* modeling of our column breakthrough curves suggests that transport of RWT is not accurately modeled as that of a single solute, as has been done in several groundwater tracer studies [e.g., *Pang and Close*, 1999; *Pang et al.*, 1998; *Sinton et al.*, 1997; *Ptak and Schmid*, 1996; *Czapar et al.*, 1994] and laboratory studies [e.g., *Everts and Kanwar*, 1994; *Kasnavia et al.*, 1999; *DiFazio and Vurro*, 1994; *Soerens and Sabatini*, 1994].

5.2. M2*i* Results

We fit M21 to BTC4 because we observe two peaks at this velocity, but it is apparent from Figure 10 that the model does not accurately represent the transport of the RWT from column experiment 4. The magnitude of the first peak is underestimated, while the magnitude of the second is overestimated. In addition, the second peak as represented by the model arrives later than the observed second peak. M21 also does not accurately fit any of the other three measured breakthrough curves.

M22, which superimposes the breakthrough curves of two solutes each modeled by M12, provides much improved results. Figure 11 shows the fit of M22 to all four breakthrough curves. At first glance, the model matches all of the data sets well with $E \approx 1 \times 10^{-5}$. With the exception of P, ω_2, and f, the parameter estimates from fitting M22 to all BTCs, except BTC4, are within 20% of each other. Note that the estimates from fitting BTC1 and BTC2 are almost identical.

M22 does not fit the data as accurately for the lower flow

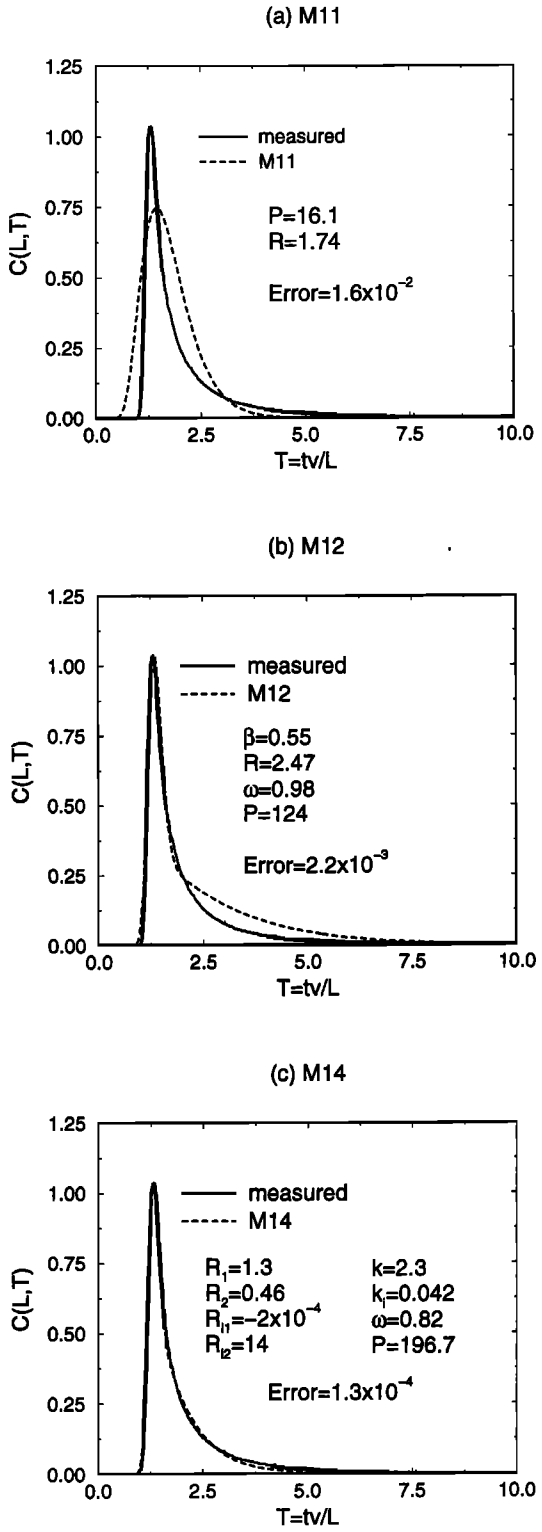

Figure 9. BTC1 ($v = 0.193$ cm s^{-1}) and the least squares fit of (a) M11, (b) M12, and (c) M14.

rates used in experiments 3 and 4. For example, a closer look at Figure 11c reveals that BTC3 shows a shoulder around $T = 1.75$ while the model does not. The inability of the model to capture this feature suggests that M22 is not an appropriate model describing RWT transport shown in BTC3. The data suggest that the two isomers are chromatographically separating, resulting in a shoulder, but the model suggests that chromatographic separation is not evident. While the model appears to accurately reproduce BTC4 (Figure 11d), the estimates of β_2 and R_2 from the fit of BTC4 are orders of magnitude different than the analogous estimates from the other fits, demonstrating that this model fit is an ill-conditioned inverse problem.

The wide variation in estimates k_1 and k_2 also demonstrates the inability of M22 to accurately model the RWT transport for BTC3 and BTC4. While fits of BTC1 and BTC2 suggest $0.012 \leq k_1 \leq 0.015$ s^{-1}, the estimates from fitting BTC3 and BTC4 are 1 and 2 orders of magnitude lower, respectively. Because the same tracer and the same sand is used in each experiment, k_1 and k_2 should remain unchanged regardless of the flow rate. According to (36), given a constant k, ω should increase with a decrease in the Darcy velocity, q. This is demonstrated in an example shown in Figure 12. Using M12, we plot three breakthrough curves with $P = 250$, $\beta = 0.74$, $R = 1.8$, $\theta = 0.4$, $q = 0.03$ cm s^{-1}, and $L = 10$, 100, and 1000 cm. Referring to (36), by increasing L we are producing the same effect as lowering q: We are increasing the residence time of the solute in the porous media. Figure 12 shows that as the residence time increases, ω increases, and the breakthrough curve approaches that produced by equilibrium sorption. However, our estimate of ω_1 for BTC4 is lower than the three estimates from column experiments with higher Darcy velocities. In addition, β_1 is lower for BTC4, which translates to less RWT undergoing equilibrium sorption. Again, this contradicts theoretical arguments that increases in residence time lead to more equilibrium sorption.

Furthermore, as seen in Figure 12, breakthrough curves resulting from a tracer sorbing near or at equilibrium have peak concentrations that arrive at a dimensionless time $T \approx R$, where R is the retardation coefficient. Otherwise, the dimensionless arrival time of the peak concentration is $1 \leq T \leq R$. Our data (Figure 8) show that the breakthrough curves from experiments with higher flow rates (and thus in nonequilibrium sorption) have first peaks that arrive later than those of the breakthrough curves from the experiments with lower flow rates (and thus in approximate equilibrium sorption). This directly conflicts with model predictions and suggests a drop in

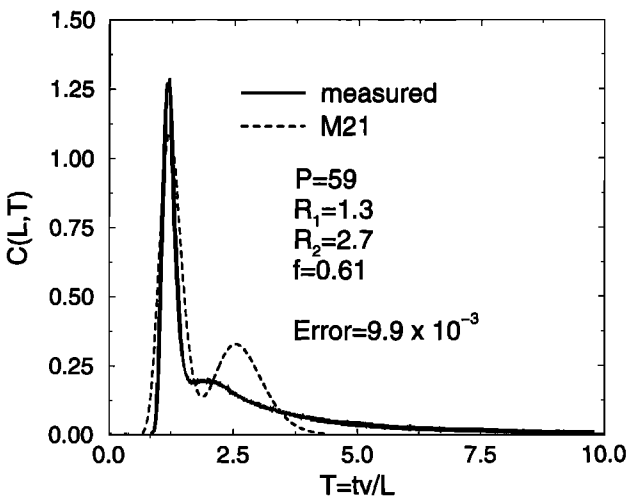

Figure 10. BTC4 ($v = 0.0117$ cm s^{-1}) and the least squares fit of M21.

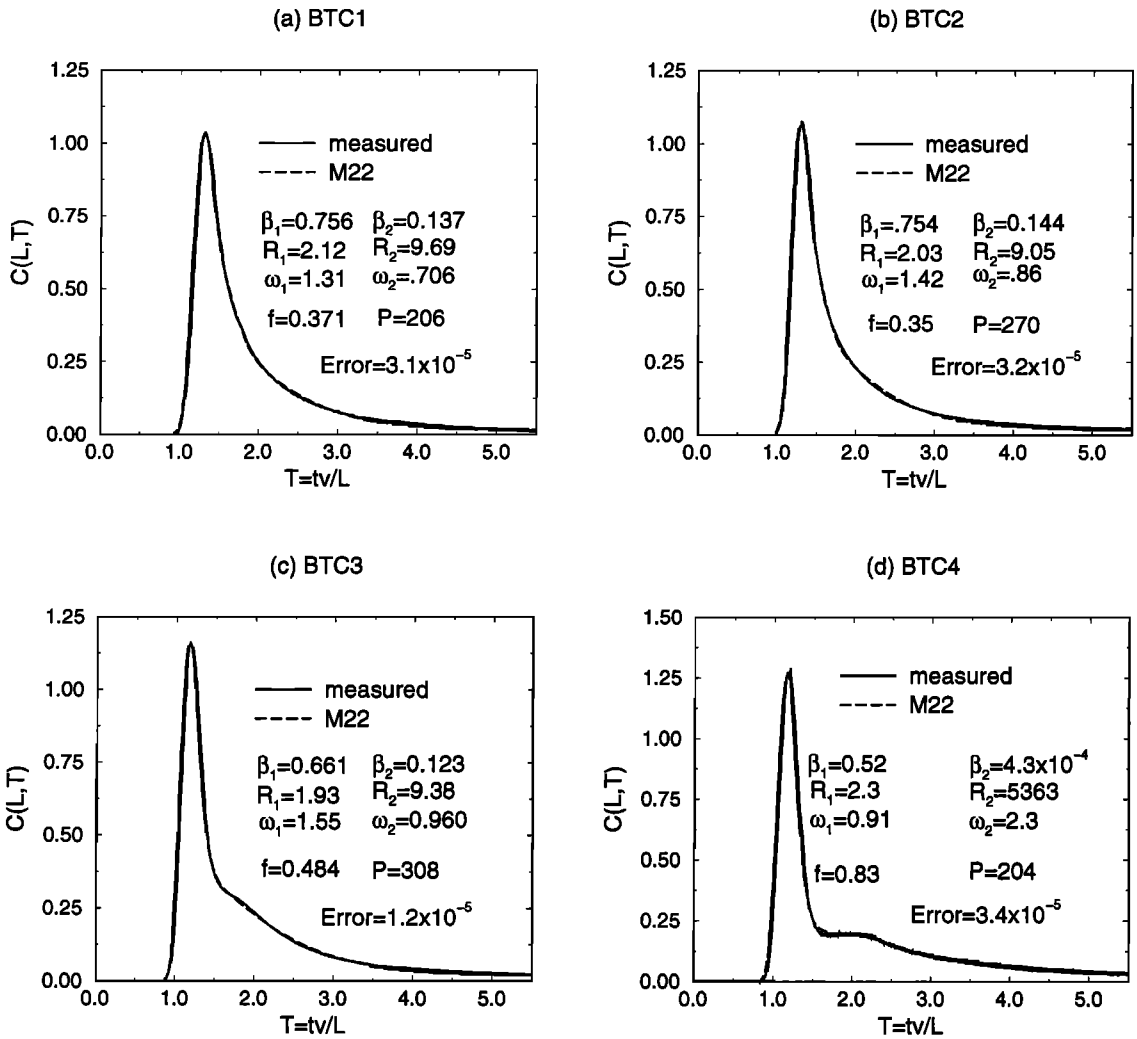

Figure 11. The least squares fits of model M22 and (a) BTC1 (v = 0.193 cm s^{-1}), (b) BTC2 (v = 0.129 cm s^{-1}), (c) BTC3 (v = 0.0175 cm s^{-1}), and (d) BTC4 (v = 0.0117 cm s^{-1}). These parameter estimates correspond to partitioning coefficients and equilibrium times summarized in Table 3.

the partitioning coefficient between column experiments conducted with high flow rates (experiments 1 and 2) and those with low flow rates (experiments 3 and 4). Between each experiment the porous medium was flushed and repacked, and we conducted a long-term procedure to recover the mass from experiment 2 which removed some of the organic material from the system. Our batch studies suggest that removal of organic material does decrease the partitioning coefficient of isomer 1 with this sand, but not to the degree needed to explain this discrepancy in the column data. Experiments 1 and 2 were conducted more than a month earlier than experiments 3 and 4. During this time the ionic composition of the water may have also changed, and according to *Everts and Kanwar* [1994] and *Sabatini and Austin* [1991], this could have an effect on the partitioning coefficient. Therefore this apparent decrease in the retardation coefficient may result from changes in the sand or water properties or possibly from experimental error. We did not measure the ionic composition of the water during these experiments, so we cannot confirm or analyze its effect on the retardation coefficient.

Because of the possible change in the properties of the material that might have occurred after BTC1 and BTC2 were measured but before BTC3 and BTC4 were obtained, we focus mainly on the parameter estimates from BTC1 and BTC2 and use BTC3 and BTC4 for more qualitative assessments of RWT transport.

The fraction of RWT that is isomer 1 should not change from experiment to experiment because the same commercial solution was used for injection. We note that the estimate of f = 0.37 and 0.35 from fitting M22 to BTC1 and BTC2 are within 10% and 20%, respectively, of the value reported by *Shiau et al.* [1993], f = 0.40. The value obtained from BTC3, f = 0.48, is also relatively close, but the value from BTC4, f = 0.83, is significantly different. However, the fraction of injected mass that is contained in the first peak of BTC4 ($0 \leq T \leq 1.4$) is 0.37, which, if the first peak only contains isomer 1, is consistent with the estimates from BTC1, BTC2, and *Shiau et al.* [1993]. This suggests that although inaccurate due to the chromatographic error, the distribution of the two isomers of RWT with a fluorometer is consistently estimated near 40% for isomer 1 and 60% for isomer 2.

The presence of isomer 2 biases the estimation of the isomer 1 parameters and f, and we suggest that this bias is stronger for BTC3 and BTC4 where the two isomers begin to appear as

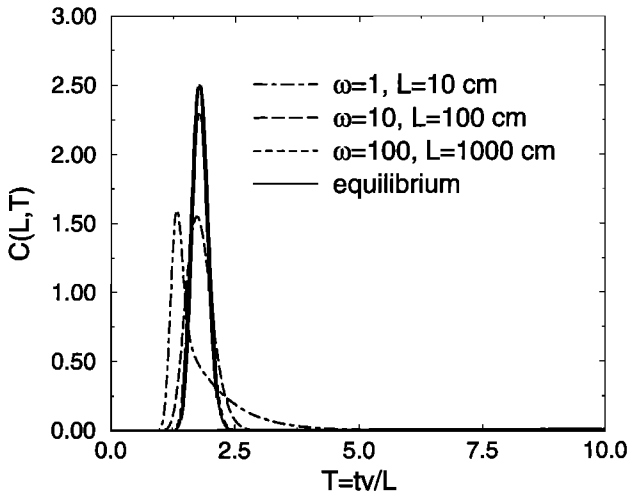

Figure 12. Simulated breakthrough curves calculated with M12 for $\omega = 1, 10$, and 100 are plotted with a breakthrough curve computed with the equilibrium sorption model. $P = 250$, $\beta = 0.74$, $\theta = 0.4$, $q = 0.03$ cm s^{-1}, and $L = 10$, 100, and 1000 cm.

distinct peaks. An explanation for a higher bias in the fits to breakthrough curves where the isomers are separating may be the inaccuracy of measuring the concentration of two individual RWT isomers with a fluorometer calibrated with the commercial-grade tracer. As discussed in section 3.3, isomer 1 and isomer 2 of RWT have different linear relationships for determining concentration from emission intensity. When the isomers are arriving as one peak, the ratio of isomer 1 to isomer 2 is closer to the ratio of the solution used for injection and for calibration of the fluorometer than it is when the isomers arrive as two distinct peaks. The largest errors will occur when the isomers arrive separately.

In an attempt to model isomer 1 from BTC4 we fit M22 to the portion of BTC4 where $0 \leq T \leq 1.3$ assuming that the contribution of isomer 2 to BTC4 is small there. The data, estimated parameters, and the breakthrough curve calculated with these parameters are shown in Figure 13. The fit is visually good, but as expected, the values for β_1, R_1, ω_1, and P are different from the estimates obtained from fitting M22 to BTC1 and BTC2, reflecting possible changes in the properties of the sand between column experiments. However, the estimated $f = 0.4$ is consistent with our column-study results and those of *Shiau et al.* [1993], both of which are biased by the chromatographic error. We note that the estimate of $k_1 = 9.33 \times 10^{-3}$ s^{-1} is much closer to the estimates from BTC1 and BTC2 than the value obtained from fitting M22 to all of BTC4, which was approximately 2 orders of magnitude lower.

Assuming the synthetic breakthrough curve plotted in Figure 13 is an accurate description of the transport of RWT isomer 1 in column experiment 4, we still need to accurately model the transport of isomer 2. We attempt this by holding constant the parameters estimated for isomer 1, f, and P while estimating β_2, R_2, and ω_2. Using M22 results in inaccurate parameters, as is evident from comparing the estimated breakthrough curve to BTC4 in Figure 14a. To find a more accurate model, we also fit M22*, this time estimating β_2, R_2, ω_2, and n_2. This result is also poor, as is evident in Figure 14b, suggesting that a nonlinear isotherm cannot describe the RWT transport at this timescale or that significant experimental error exists in this fourth column study such as a drift in the flow rate. We note that the model breakthrough curve shown in Figure 14b is not the least squares fit; rather, it represents the point at which the parameter values varied insignificantly between iterations. Trial and error model runs with various values for the parameters did not lead to a fit better than that shown in Figure 14b.

In Figure 15 we show an approximated breakthrough curve for isomer 2 generated by subtracting the estimated breakthrough curve for isomer 1 shown in Figure 13 from BTC4. The oscillation at $T \approx 1$ only represents a 2% error, as it results from fitting portions of breakthrough curves with a magnitude of $C(t)/C_0 \approx 1.25$.

6. Comparison of Column and Batch Study Results

In Table 3 we compare the estimates of K_{d1}, K_{d2}, k_1, k_2, and f as determined by the column and modeling study with the results from the batch and chemical characterization spectra studies. The parameter estimated by fitting M12 to the first peak of BTC4, as shown in Figure 13, is denoted BTC4*. To compare the kinetic batch experiments, shown in Figure 6, with the column studies, we estimate the required time for equilibrium sorption to occur. To arrive at a required time for equilibrium of isomers 1 and 2 based on the k_1 and k_2 estimates from the column study, we assume the following first-order kinetic model:

$$\frac{\partial s}{\partial t} = k_1(K_{d1}c - s) \tag{42}$$

$$c_0 = c + s \tag{43}$$

subject to

$$c(t = 0) = c_0 \qquad s(t = 0) = 0, \tag{44}$$

where $s(t)$ and $c(t)$ are the time-varying mass fraction of sorbate to sorbent and aqueous concentration, respectively, of RWT isomers 1 or 2. Solving the above system yields

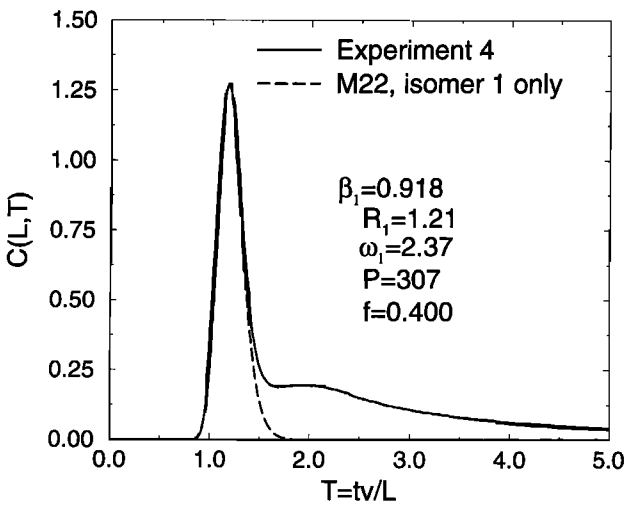

Figure 13. BTC4 ($v = 0.0117$ cm s^{-1}) and the least squares fit of M22 for isomer 1 to the portion of BTC4 where $0 \leq T \leq 1.3$. These parameter estimates correspond to $K_1 = 0.060$ cm^3 g^{-1}, $F_{e1} = 0.528$, and $k_1 = 9.33 \times 10^{-3}$ s^{-1}.

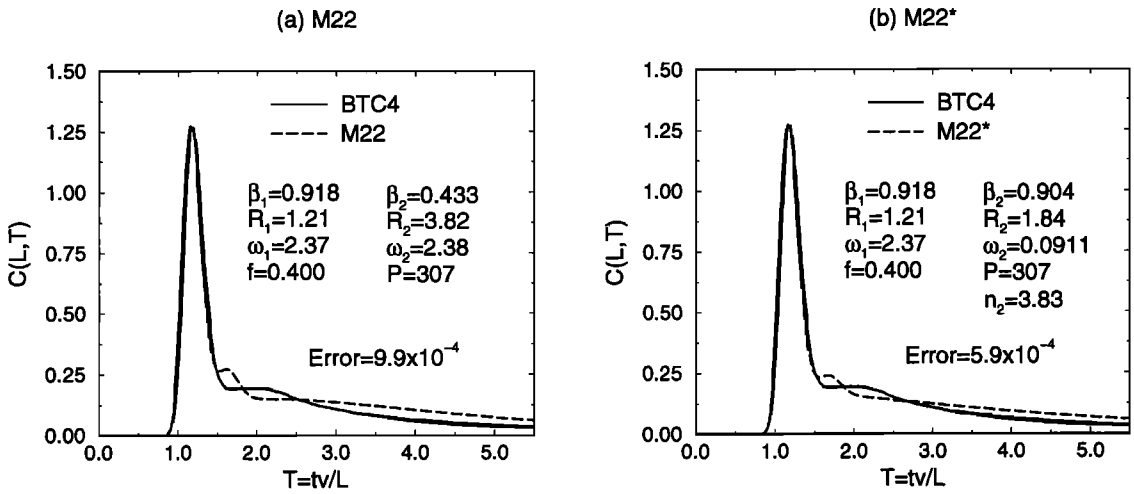

Figure 14. BTC4 and a synthetic breakthrough curve obtained by fitting (a) M22 and (b) M22* to BTC4. Here β_2, R_2, and ω_2 are the only variable parameters for the M22 fit, while those and n_2 are the only variable parameters for the M22* fit. All other parameters are equal to the estimates obtained from fitting M22 to the portion of BTC4 where $0 \leq T \leq 1.3$.

$$s(t) = \frac{K_{d1}c_0}{K_d + 1}(1 - e^{-k_1 t}). \quad (45)$$

When $t = k_1/3$, $s(t)$ is approximately 95% of the equilibrium value. We therefore define the approximate times to equilibrium for isomers 1 and 2 as $\tau_1 = 3/k_1$ and $\tau_2 = 3/k_2$, respectively. We note that the time to equilibrium sorption of isomer 1 to the treated and untreated sand in the batch study cannot be accurately determined from our results due to insufficient resolution. However, equilibrium appears to have been reached by the time our first (5-min) measurements were made (Figure 6). For the batch experiments we therefore select $\tau_1 \approx 5$ min as the time isomer 1 takes to reach equilibrium sorption on both the treated and untreated sand.

The high values of τ_1, τ_2, and f for BTC3 and BTC4 as well as the high value of K_{d2} for BTC4 relative to the values estimated from BTC1, BTC2, and the batch and chemical characterization studies suggest that M22 does not accurately describe the RWT transport in BTC3 and BTC4. This and the estimate of $K_{d2} = 1532$ cm^3 g^{-1} for BTC4 (Table 3) illustrate the danger of using an incorrect model for parameter estimation. If the partitioning coefficient of the sand for BTC4 is allowed to drop to 0.060 cm^3 g^{-1} and M12 is used to fit the first peak of BTC4 (BTC4*), the values of τ_1 and f agree with the other results. This reconfirms our hypothesis that the properties of the column sand sample changed between column experiments. Therefore, as mentioned before, we do not consider the parameter estimates from BTC3 and BTC4 but, rather, use these breakthrough curves for their qualitative information. They illustrate the chromatographic effect, that is, separation of the two RWT isomers as they are transported through subsurface material.

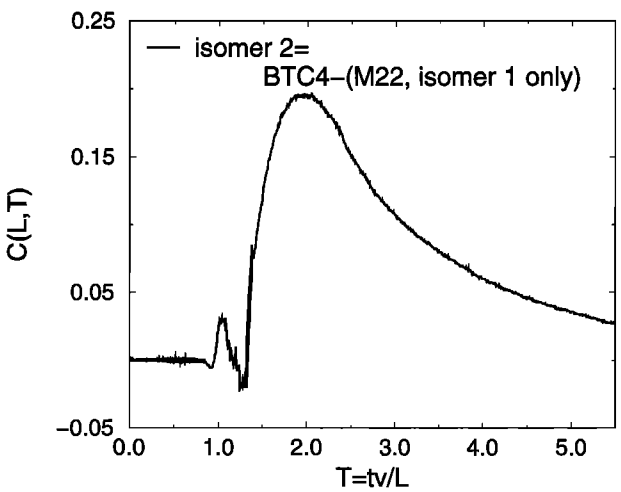

Figure 15. An estimate of the contribution of isomer 2 to BTC4 obtained from subtracting estimated breakthrough curve for isomer 1 from BTC4. The oscillation at $T = 1$ represents a smaller error, as the magnitude of the first peak of BTC4 is approximately 1.25.

The estimates of K_{d1} from BTC1 and BTC2 are in excellent agreement with the values from the batch experiments for the untreated sand as seen from Table 3. The estimates for K_{d2} from BTC1, BTC2, and the batch experiments are of the same order of magnitude. BTC1, BTC2, BTC4*, and the batch experiments also yielded similar results for the approximate time required to equilibrium sorption.

When we discussed the fit of M22 to the BTCs, we mentioned that the column-study estimates of f, and the related distribution ratio of the two isomers, obtained by us and by *Shiau et al.* [1993] are biased due to the chromatographic error. However, a chromatographic error of approximately 20% is required to reconcile the 40/60 isomer distribution ratio suggested by those column studies with the 50/50 one estimated in our chemical characterization study.

7. Extrapolation to the Field Scale

As the timescale of advection increases sufficiently beyond the timescale of the sorption, a model accounting only for equilibrium sorption becomes more accurate. For simplicity, we only analyze the sorption timescale of isomer 1. Revisiting

Table 3. Comparison of Parameter Estimates From the Column and Modeling Study With Those From the Batch and Chemical Characterization Studies

	K_{d1}, cm^3 g^{-1}	K_{d2}, cm^3 g^{-1}	τ_1, min	τ_2, min	f
BTC1	0.320	2.48	3.1	92	0.35
BTC2	0.294	2.30	4.1	105	0.37
BTC3	0.266	2.39	36	796	0.48
BTC4	0.37	1532	156	2.9×10^5	0.83
BTC4*	0.060	N/A	5.4	N/A	0.40
Batch (treated)	0.187	1.48	~5	60–120	
Batch (untreated)	0.313	1.55	~5	>24 hours	
Chemical characterization					~0.50

BTC4* refers to the parameter estimates obtained from fitting M12 to the early portion of BTC4, as shown in Figure 13. The rate constants k_1 and k_2 are replaced by approximate time, in minutes, required for equilibrium sorption, τ_1 and τ_2. Subscripts 1 and 2 refer to rhodamine WT isomers 1 and 2, respectively. N/A, not available.

(36), we note that ω is a dimensionless parameter describing the rate of the exchange of a RWT isomer between the system water and the soil sample. As is evident in (36), ω is a dimensionless rate constant composed of a factor, $k_1(1 - F_{e1})\rho K_{d1}$, with units of $1/s$ and scaled by an advective timescale L/q, where L is a characteristic length and q is the Darcy velocity. In effect, ω is a ratio of the advective timescale over the sorption timescale. Revisiting Figure 12, we note that the arrival time of the peak concentration of a breakthrough curve resulting from nonequilibrium sorption is equal to that of a breakthrough curve resulting from equilibrium sorption if ω is sufficiently high. In the case of the parameters used to calculate the breakthrough curves in Figure 12, $\omega \geq 10$ is sufficiently high. The corresponding travel time to $\omega \geq 10$ is $RL\theta/q \geq 2400$ s. These parameters are similar to those estimated from fitting M22 to BTC1 and BTC2. Therefore, if our parameter estimates for RWT isomer 1 are correct, then the equilibrium sorption model should estimate accurately the peak arrival time of isomer 1 transport through our sand when the travel time exceeds approximately 40 min. However, for the equilibrium sorption model to accurately describe the entire breakthrough curve, the travel time should exceed approximately $L\theta/q \geq 6 \times 10^4$ s (~400 min).

Furthermore, at a residence time of approximately 50 min (BTC4) we have seen that an RWT breakthrough curve contains two overlapping peaks. A concentration breakthrough curve from a tracer test with RWT that contains two peaks may be ambiguous in that the two peaks may result from a heterogeneity in the hydraulic conductivity or the two isomers arriving at different times. Given the difficulty in modeling the transport of isomer 2 in a column study, a tracer test should be conducted on a sufficiently large timescale for the two isomers to arrive as distinct peaks.

To illustrate the ambiguity that arises from using commercially available RWT in small-scale tracer tests, we present in Figure 16 the breakthrough curve from a small-scale, single-borehole tracer test called the dipole-flow test with a tracer (DFTT) conducted on the length scale of approximately 1 m in well L-32 at the Lizzie field site near Greenville, North Carolina [*Sutton et al.*, 2000]. The first peak and shoulder that arrive in approximately 15 and 40 min are likely due to heterogeneities in the hydraulic conductivity of the aquifer, while the peak and shoulder at approximately 70 and 120 min are likely due to isomers 1 and 2 arriving at different times. The presence of both RWT isomers complicates the interpretation of this breakthrough curve, and those unaware that RWT contains two isomers may mistake these two later peaks for aquifer heterogeneity. For the signals of isomers 1 and 2 to arrive separately, the timescale of the test may need to be increased by an order of magnitude, which is inconvenient given that this test took over 5 hours. If the timescale of the tracer test is increased sufficiently, the signal of isomer 2 may never be recorded. In such a case, it is important to note that only 40–50% of the injected mass will be recovered.

8. Conclusions

We conducted chemical characterization, batch, column, and modeling studies to elucidate the sorption and transport of rhodamine WT (RWT) in the subsurface. As a representative porous media, we selected the sand used to fill the sand packs around the monitoring wells at the Lizzie field site near Greenville, North Carolina. The chemical characterization study involved separating the constituents of commercially available RWT and analyzing them with UV and fluorescence detection. We confirmed that there are two isomers of RWT and found that they have distinct emission spectra. The batch study involved experiments to analyze the sorption (kinetics and isotherms) of both RWT isomers to the original sand sample and to a sample with the organic material removed. To interpret the breakthrough curves from our four column experiments,

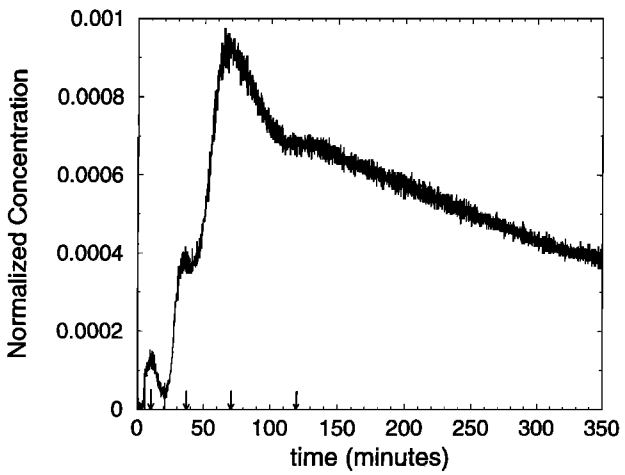

Figure 16. Data from a dipole-flow test with a tracer conducted with RWT [*Sutton et al.*, 2000] showing both heterogeneities and possibly the partially overlapping signals of isomers 1 and 2. Arrows on the time axis denote the arrival times of the peaks and shoulders.

we fit them with six reactive-solute transport models of varying complexity. Three of the models, taken from existing literature, account only for a single solute. The other three models, which we propose in this paper, combine two single-solute models to account for the two RWT isomers.

We did find an inconsistency between the transport models and our data. This discrepancy is likely due, in part, to (1) a change in the properties of the sand from flushing and repacking of the column between experiments, (2) possible experimental errors in measuring flow rate or variations in the ionic composition of the system water, and (3) the chromatographic error that we introduce in this paper. Analyzing the results from our chemical characterization, batch, column, and modeling studies and accepting this discrepancy with the data, we arrive at the following conclusions about the properties of RWT and its sorption to the porous media we used.

1. We established the distinct emission fluorescence spectra of the two isomers of RWT and confirmed the finding of *Shiau et al.* [1993] that the two isomers have distinct sorption properties. The identical fluorophore structures and nearly identical intensities at the emission-spectra maxima of the two isomers strongly suggest a 50/50 isomer ratio in commercially available RWT.

2. One isomer of RWT (isomer 1) sorbs to a lesser extent and reaches equilibrium sorption an order of magnitude faster than the other isomer (isomer 2). We also found that a linear isotherm describes the partitioning of isomer 1, while a Freundlich isotherm describes the partitioning of isomer 2.

3. The different emission spectra and sorption properties of the two isomers of RWT complicate the use of a fluorometer to accurately measure the concentration of commercially available RWT. As the two isomers travel through the subsurface, they separate, changing their relative concentrations in solution. As the relative concentrations depart from those used to calibrate the fluorometer, the error in the concentration measurement may increase up to approximately 7.8%. This error has biased our parameter estimates and may affect interpretation of field tracer tests.

4. Through column studies with a fluorometer, we and *Shiau et al.* [1993] independently estimated a 40/60 ratio of isomer 1 to isomer 2. This estimate, however, is likely biased, because a fluorometer does not account for the different emission spectra of the two isomers. The chromatographic error we have measured is not sufficiently large to fully account for the discrepancy between this estimate and the 50/50 one we obtained by considering the isomer structures and emission spectra.

5. For the transport timescales tested, none of the models that consider a single solute can accurately describe the RWT transport. While the model proposed by *Brusseau et al.* [1989] does reproduce the two breakthrough curves with a single peak, the parameter estimates are unrealistic.

6. A model (M22 in the text) that considers two RWT isomers sorbing noncompetitively to equilibrium and nonequilibrium sorption sites following linear isotherms accurately describes the transport of RWT on short timescales through our porous media sample. Furthermore, parameter estimates from fitting this model to short-timescale breakthrough curves are similar to estimates obtained from batch studies. Neither the M22 model, nor its modification (M22* in the text) that allows for a Freundlich isotherm for one isomer, can accurately describe the transport of both isomers of RWT through our porous media for experiments conducted with longer timescales.

7. A single-solute, two-site model that accounts for nonequilibrium sorption (M12 in the text) can accurately describe the transport of RWT isomer 1 at a variety of timescales.

8. The presence of the two RWT isomers complicates the interpretation of field tracer tests, because a shoulder or any two peaks in a breakthrough curve may be caused by either heterogeneity in the aquifer hydraulic conductivity or the different arrival times of the two isomers. In some cases, isomer 2 may sorb to such an extent that its breakthrough is not recorded during a test, allowing only isomer 1 to be measured. In such cases, only about 50% of the injected mass may be recorded.

On the basis of the above conclusions, we find that RWT isomer 1 would be an excellent groundwater tracer that sorbs to a relatively small degree and can be modeled relatively easily. Contrastingly, we find that RWT isomer 2 is a poor groundwater tracer that sorbs to a relatively large extent and follows a nonlinear isotherm. The effectiveness of commercially available RWT is hampered by the presence of both isomers because (1) they have different sorption properties and emission spectra that introduce errors into RWT concentration measurements made with a field fluorometer, (2) isomer 2 sorption follows a nonlinear Freundlich isotherm that complicates the modeling of RWT transport, and (3) tracer tests that result in breakthrough curves with two peaks are ambiguous given that the peaks could be caused by either heterogeneities in hydraulic conductivity or by the different arrival times of the two isomers. We therefore suggest that efforts be made to separate the two isomers and provide RWT solutions that contain isomer 1 as the only active ingredient.

Acknowledgments. We thank Xiao Zhuang and Ryan L. Fimmen from Duke's Nicholas School of the Environment for developing the HPLC method for RWT isomer separation and assisting with the studies. This research was partially supported by the U.S. Geological Survey, USGS agreement 1434-HQ-96-GR-02689; the North Carolina Water Resources Research Institute, WRRI project 70165; the National Science Foundation under grant DMS-9873275; and the National Institute of Environmental Health Sciences under grant 1P42-ES-10356-01. It was performed while D. J. Sutton and Z. J. Kabala were graduate student and faculty advisor, respectively, in the Department of Civil and Environmental Engineering at Duke University and while D. Vasudevan and A. Francisco were faculty advisor and graduate student, respectively, in Duke's Nicholas School of the Environment.

References

Adams, E. E., and L. W. Gelhar, Field study of dispersion in a heterogeneous aquifer, 2, Spatial moments analysis, *Water Resour. Res.*, *28*(12), 3293–3307, 1992.

Bencala, K. E., R. E. Rathbun, A. P. Jackman, V. C. Kennedy, G. W. Zellweger, and R. J. Avanzino, Rhodamine WT dye losses in a mountain stream environment, *Water Resour. Bull.*, *19*(6), 943–950, 1983.

Brusseau, M. L., R. E. Jessup, and P. S. C. Rao, Modeling the transport of solutes influenced by multiprocess nonequilibrium, *Water Resour. Res.*, *25*(9), 1971–1988, 1989.

Cameron, D. A., and A. Klute, Convective-dispersive solute transport with a combined equilibrium and kinetic adsorption model, *Water Resour. Res.*, *13*(1), 183–188, 1977.

Czapar, G. F., R. S. Kanwar, and R. S. Fawcett, Herbicide and tracer movement to field drainage tiles under simulated rainfall conditions, *Soil Tillage Res.*, *30*(1), 19–32, 1994.

Datta-Gupta, A., L. W. Lake, G. A. Pope, and M. J. King, A type-curve

approach to analyzing 2-well tracer tests, *SPE Form. Eval.*, *10*(1), 40–48, 1995.

Derouane, J., and A. Dassargues, Delineation of groundwater protection zones based on tracer tests and transport modeling in alluvial sediments, *Environ. Geol.*, *36*(1-2), 27–36, 1998.

DiFazio, A., and M. Vurro, Technical note: Experimental tests using rhodamine WT as tracer, *Adv. Water Resour.*, *17*(6), 375–378, 1994.

Everts, C. J., and R. S. Kanwar, Evaluation of rhodamine WT as an adsorbed tracer in an agricultural soil, *J. Hydrol.*, *153*(1-4), 53–70, 1994.

Field, M. S., R. G. Wilhelm, J. F. Quinlan, and T. J. Aley, An assessment of the potential adverse properties of fluorescent tracer dyes used for groundwater tracing, *Environ. Monit. Assess.*, *38*(1), 75–96, 1995.

Garbow, B. S., K. E. Hillstrom, and J. J. More, *Minpack Project*, Argonne Natl. Lab., Argonne, Ill., 1980.

Gelhar, L. W., and M. A. Collins, General analysis of longitudinal dispersion in nonuniform flow, *Water Resour. Res.*, *7*(6), 1511–1521, 1971.

Grove, D. B., and B. Beetem, Porosity and dispersion constant calculations for a fractured carbonate aquifer using a two well tracer method, *Water Resour. Res.*, *7*(1), 128–134, 1971.

Hess, K. M., S. H. Wolf, and M. A. Celia, Large-scale natural gradient tracer test in sand and gravel, Cape Cod, Massachusetts, 3, Hydraulic conductivity variability and calculated macrodispersivities, *Water Resour. Res.*, *28*(8), 2011–2027, 1992.

Hofstraat, M. S., G. Vriezekolk, W. Schreurs, G. J. A. A. Broer, and N. Wijnstok, Determination of rhodamine WT in surface water by solid-phase extraction and HPLC with fluorescence detection, *Water Res.*, *25*(7), 883–890, 1991.

Jury, W. A., W. R. Gardner, and W. H. Gardner, *Soil Physics*, 5th ed., John Wiley, New York, 1991.

Kasnavia, T., D. Vu, and D. A. Sabatini, Fluorescent dye and media properties affecting sorption and tracer selection, *Ground Water*, *37*(3), 376–381, 1999.

Kass, W. A., Hydrological tracing practice on underground contaminations, *Environ. Geol.*, *23*, 23–29, 1994.

Mackay, D. M., D. L. Freyburg, P. V. Roberts, and J. A. Cherry, A natural gradient experiment on solute transport in a sand aquifer, 1, Approach and overview of plume movement, *Water Resour. Res.*, *22*(13), 2017–2029, 1986.

Nkedi-Kizza, P., J. W. Biggar, H. M. Selim, M. T. van Genuchten, P. J. Wierenga, J. M. Davidson, and D. R. Nielsen, On the equivalence of two conceptual models for describing ion exchange during transport through an aggregated oxisol, *Water Resour. Res.*, *20*(8), 1123–1130, 1984.

Pang, L., and M. Close, Field-scale physical non-equilibrium transport in an alluvial gravel aquifer, *J. Contam. Hydrol.*, *38*, 447–464, 1999.

Pang, L., M. Close, and M. Noonan, Rhodamine WT and *Bacillus subtilis* transport through an alluvial gravel aquifer, *Ground Water*, *36*(1), 112–122, 1998.

Ptak, T., and G. Schmid, Dual-tracer transport experiments in a physically and chemically heterogeneous porous aquifer: Effective transport parameters and spatial variability, *J. Hydrol.*, *183*(1-2), 117–138, 1996.

Sabatini, D. A., and T. A. Austin, Characteristics of rhodamine WT and fluroescein as adsorbing ground-water tracers, *Ground Water*, *29*(3), 341–349, 1991.

Selim, H. M., J. M. Davidson, and R. S. Mansell, Evaluation of a two-site adsorption-desorption model for describing solute transport in soils, in *Proceedings, Summer Computer Simulation Conference*, p. 444, Natl. Sci. Found., Washington, D. C., 1976.

Shiau, B., D. A. Sabatini, and J. H. Harwell, Influence of rhodamine WT properties on sorption and transport in subsurface media, *Ground Water*, *31*(6), 913–920, 1993.

Sinton, L. W., R. K. Finlay, L. Pang, and D. M. Scott, Transport of bacteria and bacteriophages in irrigated effluent into and through an alluvial gravel aquifer, *Water Air Soil Pollut.*, *98*(1-2), 17–42, 1997.

Smart, P. L., and I. M. S. Laidlaw, An evaluation of some fluorescent dyes for water tracing, *Water Resour. Res.*, *13*(1), 15–33, 1977.

Soerens, T. S., and D. A. Sabatini, Cosolvency effects on sorption of a semipolar, ionogenic compound (rhodamine WT) with subsurface materials, *Environ. Sci. Technol.*, *28*(6), 1010–1014, 1994.

Sutton, D. J., Z. J. Kabala, D. E. Schaad, and N. C. Ruud, The dipole-flow test with a tracer: A new single-borehole tracer test for aquifer characterization, *J. Contam. Hydrol.*, *44*, 71–101, 2000.

Talbot, A., The accurate numerical inversion of Laplace transforms, *J. Inst. Math Its. Appl.*, *23*(1), 97–120, 1979.

Trudgill, S. T., Soil water dye tracing with special reference to the use of rhodamine WT, lissamine FF and amino G acid, *Hydrol. Process.*, *1*, 149–170, 1987.

Turner Designs, Inc., *A Practical Guide to Flow Measurements*, a monograph, Sunnyvale, Calif., 1998a.

Turner Designs, Inc., *Model 10-AU-005-CE Fluorometer User's Manual*, part number 10-AU-074, Sunnyvale, Calif., June 1998b.

Valocchi, A. J., Validity of the local equilibrium assumption for modeling sorbing solute transport through homogeneous soils, *Water Resour. Res.*, *21*(6), 808–820, 1985.

van Genuchten, M. T., and P. J. Wierenga, Mass transfer studies in sorbing porous media, I, Analytical solutions, *Soil Sci. Soc. Am. J.*, *40*, 473–480, 1976.

van Genuchten, M. T., and P. J. Wierenga, Mass transfer studies in sorbing porous media, II, Experimental evaluation with tritium (^3H_2O), *Soil Sci. Soc. Am. J.*, *41*, 272–277, 1977.

Welty, C., and L. W. Gelhar, Evaluation of longitudinal dispersivity from nonuniform flow tracer tests, *J. Hydrol.*, *153*, 71–102, 1994.

A. Francisco and D. Vasudevan, Nicholas School of the Environment, Duke University, Box 90328, Durham, NC 27708.

Z. J. Kabala and D. J. Sutton, Department of Civil and Environmental Engineering, Duke University, Box 90287, Durham, NC 22708. (kabala@copernicus.egr.duke.edu)

(Received January 24, 2000; revised August 9, 2000;
accepted September 20, 2000.)